frontiers in Materials

ORIGINAL RESEARCH
published: 25 February 2021
doi: 10.3389/fmats.2020.619315

Multilayer Maraging/CoCrNi Composites With Synergistic Strengthening-Toughening Behavior

C. X. Chen[1,2,3], *Y. F. Ge*[1,2,3], *W. Fang*[1,2,3]*, *X. Zhang*[1,2,3], *B. X. Liu*[1,2,3]*, *J. H. Feng*[1,2,3] and *F. X. Yin*[1,2,3]

[1]Research Institute for Energy Equipment Materials, Hebei University of Technology, TianJin, China, [2]TianJin key laboratory of Materials laminating Fabrication and Interfacial Controlling Technology, Hebei University of Technology, TianJin, China, [3]School of Materials Science and Engineering, Hebei University of Technology, TianJin, China

A novel multilayer maraging/CoCrNi composite with good mechanical properties was successfully fabricated by a vacuum hot-rolling and aging treatment. The yield strength, tensile strength, uniform elongation, and fracture elongation reached 1,151, 1,380 MPa, 15.7, and 24% respectively, realizing the aim of synergistic strengthening–toughening by effectively improving the yield strength of the CoCrNi alloy and strain-hardening capacity of the maraging steel. The vacuum state, high rolling reduction ratio, and alloy element diffusion are beneficial in strengthening the clad interface. The good work-hardening capacity of the CoCrNi alloy compensates for the poor strain-softening behavior of the maraging steel, effectively delaying the premature localized necking of the multilayer composites. The strengthening–toughening mechanism of the multilayer maraging/CoCrNi composites is mainly attributed to the strong interface, nanoscale precipitation, and strain-induced twinning.

Keywords: multilayer composites, CoCrNi alloy, work hardening capacity, vacuum hot rolling, synergistic deformation capacity

OPEN ACCESS

Edited by:
Minghui Cai,
Northeastern University, China

Reviewed by:
Gm Xie,
Northeastern University, China
Xiping Cui,
Harbin Institute of Technology, China

***Correspondence:**
W. Fang
fangwei@hebut.edu.cn
B. X. Liu
liubaoxi@hebut.edu.cn

Specialty section:
This article was submitted to Structural Materials, a section of the journal Frontiers in Materials

Received: *20 October 2020*
Accepted: *04 November 2020*
Published: *25 February 2021*

Citation:
Chen CX, Ge YF, Fang W, Zhang X, Liu BX, Feng J H and Yin FX (2021) Multilayer Maraging/CoCrNi Composites With Synergistic Strengthening-Toughening Behavior. Front. Mater. 7:619315. doi: 10.3389/fmats.2020.619315

INTRODUCTION

High-strength metals always display low ductility, toughness, and strain-hardening capacity, while ductile metals exhibit low yield strength and tensile strength, which seriously limits their practical applications (Lesuer et al., 1996; Yin et al., 2013; Jing et al., 2014; Zhang et al., 2014; Seok et al., 2016; Liu et al., 2019). Recently, multilayer metals containing different constituent metallic layers were reported to show outstanding comprehensive mechanical properties (Inoue et al., 2008; Ojima et al., 2012; Kang et al., 2016; Ding et al. 2018; Yu et al., 2018; Chang et al., 2019; Ding et al., 2021). For example, a novel multilayer twinning-induced plasticity (TWIP)/maraging steel with a tensile strength of 1,527 MPa and a fracture elongation of 21.5% was successfully fabricated by Yu et al. (2018). However, the TWIP layer could not compensate for the poor strain-softening behavior of the maraging steel layer, which leads readily to negative strain hardening of the multilayer steel. In the present study, a novel CoCrNi alloy with superior strain-hardening capacity was chosen to replace the TWIP steel layer, giving the CoCrNi alloy an excellent combination of tensile strength and ductility (Slone et al., 2018). Moreover, different from high manganese steel with a martensitic transformation, the CoCrNi alloy maintains the original face-centered cubic structure by forming twins (Grassel et al., 2000; Gutierrezurrutia and Raabe, 2011; Wu et al., 2014; Miao et al., 2017; Slone et al., 2018; Slone et al., 2019). We demonstrate a novel approach

TABLE 1 | The chemical composition of C300 maraging steel and CoCrNi medium-entropy alloy (wt%).

Element	Mn	Si	Al	C	Ni	Co	Mo	Ti	Fe	Cr
C300	≤0.1	≤0.1	0.1	≤0.03	18.0	9.0	5.0	0.7	67.2	—
CoCrNi	—	—	—	—	34.61	34.74	—	—	—	30.65

to overcoming the strengthening–toughening limit and delaying localized necking, which can provide a means of researching multilayer metal matrix composites.

MATERIALS AND METHODS

Two very different kinds of metals were used as the raw materials in this study. One is maraging steel (C300), which has superior yield strength and poor strain-softening behavior, while the other is a CoCrNi alloy, which has excellent fracture elongation and a low yield strength. The chemical compositions of the C300 maraging steel and the CoCrNi alloy are listed in **Table 1**. The C300 maraging steel and CoCrNi high-entropy alloy(HEA) were cut into thin plates with a thickness of 0.5 mm and a diameter of 48 mm by wire cutting. Then, the plates were alternately stacked to give a total of 60 layers, and the stacked plates were sealed into a carbon steel box under vacuum of 10^{-2} Pa. Subsequently, the box was heated at 1,200°C for 30 min, and then hot rolled to a final thickness of 4 mm (**Figure 1C**). After rolling, some specimens were cut from the hot-rolling multilayer maraging/CoCrNi composite and finally heated at 485°C for 4 h.

The microstructure and distribution of the alloying elements were examined by optical microscopy (OM), electron back-scattering diffraction (EBSD), scanning electron microscopy, electron probe microanalysis (EPMA), and transmission electron microscopy. The dog-bone tensile samples with a gauge length of 18 mm and a width of 3 mm were tested using an AGS 50 KN universal testing machine. The strain distribution and evolution were tested and recorded using a digital image correlation (DIC) method equipped with a contactless full-field strain-measuring system.

RESULTS AND DISCUSSION

The EBSD microstructures of the individual CoCrNi alloy and C300 maraging steel are shown in **Figures 1A,B**. Obviously, the CoCrNi alloy has rather coarse as-cast columnar grains with an average size of 500 μm, and the C300 maraging steel has a coarse lath-like martensite microstructure. The OM microstructures of the hot-rolled and aged samples are shown in **Figures 1D,E**. The straight clad interfaces and uniform layer with a thickness of approximately 65 μm can be clearly seen, which indicates that the two constituent alloys have superior deformation coordination capacity during the hot-rolling process.

Figure 2 shows the EBSD microstructure and EPMA mapping of the multilayer maraging/CoCrNi composites. After hot rolling, the grains of the individual layers were obviously refined compared with the original grains, and the average grain size of the CoCrNi layer and lath spacing of the C300 layers are about 5 and 3 μm, respectively. In addition, the grain orientations in the CoCrNi layers are relatively random, while the maraging layer shows an obvious <110>//RD texture. **Figures 2A–C** shows that many ultrafine grains appear along the clad interface, which is due to a high rolling reduction ratio and sufficient alloying element diffusion. This can also lead to the formation of a transition layer with a thickness of 3 μm. Additionally, **Figure 2D** shows that nanoscale rod-like precipitates with a length of 20 nm and width of 5 nm appear in the C300 layer after the aging treatment. Specifically, the precipitates are identified as the η-Ni_3Ti phase, as shown by the electron diffraction pattern in **Figure 2E**. This phase can effectively strengthen the C300 layers. Also, many microscale Al_2O_3 phases appear at the transition layer owing to the high Al content and surface oxidation in the C300 layer. Deformation twins are also generated in the CoCrNi layer, which is similar to the TWIP effect during the hot-rolling process (He et al., 2020). According to EPMA mapping scanning analysis, as shown in **Figure 2I–L**, many fine Al_2O_3 and TiN particles are located at the transition interface. Herein, the formation of Al_2O_3 and TiN is attributed to the selection of oxidation and nitridation at the surface of the C300 maraging steel layer. That is to say, a high vacuum of 10^{-2} Pa still cannot prevent the oxidation and nitridation of Al and Ti because of their strong chemical activity.

Figure 3 shows the tensile behavior and DIC whole-field strain distribution of the individual materials and multilayer C300/

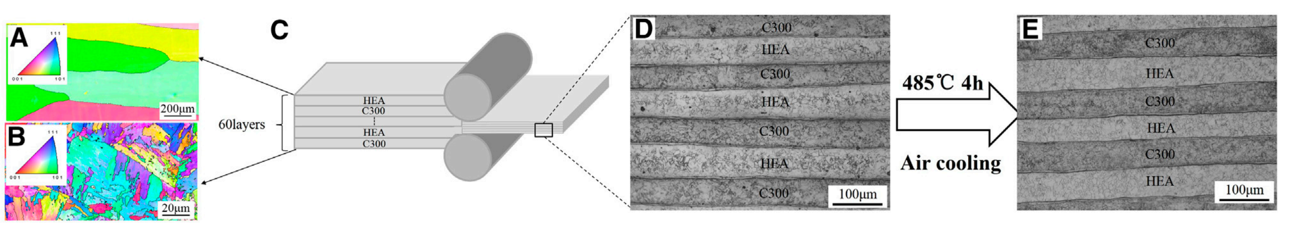

FIGURE 1 | (A,B) Inverse pole figure the IPF mapping of original the original CoCrNi alloy and C300. **(C)** a schematic diagram of the hot-rolling process, **(D,E)** the optical microstructures of the hot-rolled and aged multilayer maraging/CoCrNi composite.

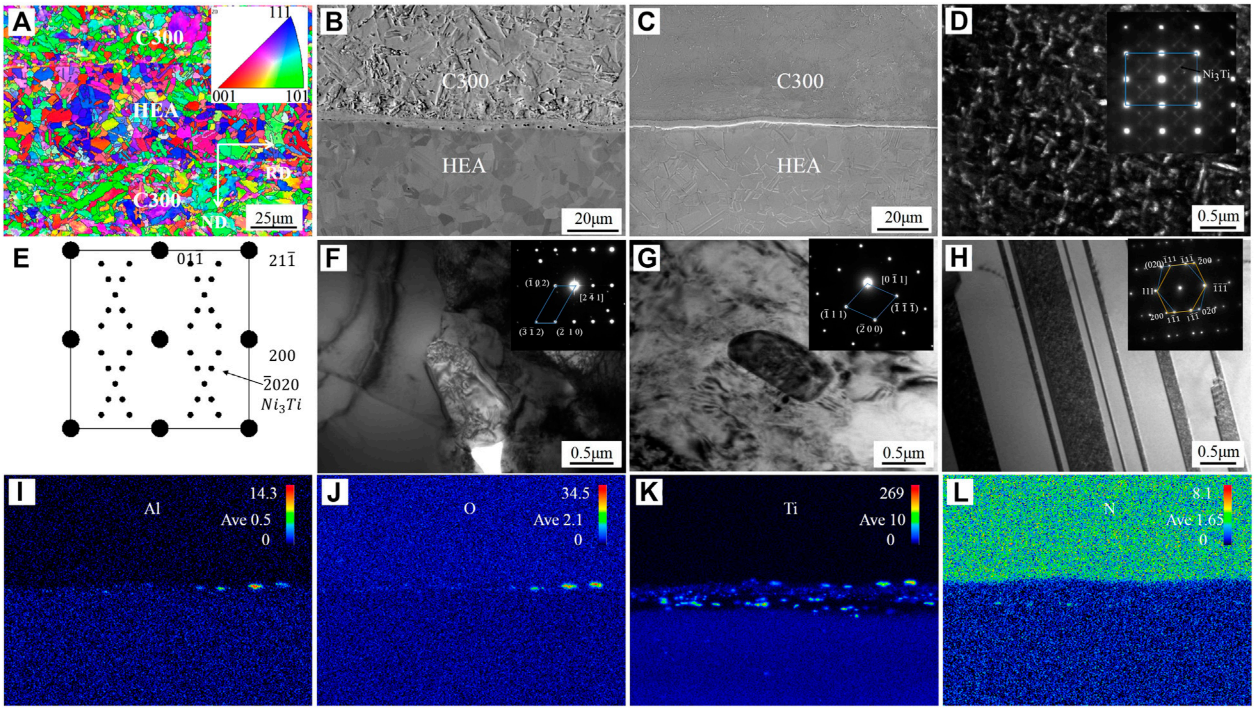

FIGURE 2 | (A) Electron back-scattering diffraction maps of the rolled multilayer maraging/CoCrNi composites. RD indicates the rolling direction and ND the normal direction. **(B)** Scanning electron microscopy (SEM) of hot-rolled sample. **(C)** SEM of an aged sample. **(D) (F) (G) (H)** Transmission electron microscopy of Ni_3Ti, Al_2O_3, TiN and twinning of aged multilayer maraging/CoCrNi composite; **(E)** Indexing of diffraction pattern illustration of **D**; **(I–L)** EPMA mapping distribution of an aged sample.

CoCrNi composites. Herein, the individual CoCrNi alloy has a high work-hardening capacity, a superior tensile fracture elongation of 50%, and a rather low yield strength of 269 MPa, as shown in **Figures 3A,B**. However, the individual C300 maraging steel reveals a superior yield strength of 1951 MPa, poor strain-softening behavior, and a poor work-hardening rate. Based on the above multilayer design idea, a relatively high tensile strength of 855 MPa and a uniform elongation of 21.7% can be obtained for the hot-rolled C300/CoCrNi multilayer composites. Moreover, after the aging treatment, the composites obtained a superior tensile strength of 1,380 MPa and a superior fracture elongation of 24% (uniform elongation of 15.7%). Here, the strengthening mechanisms of the multilayer metal matrix composites are mainly attributed to grain refining, strain-induced twinning, and nanometer precipitate strengthening. Noticeably, the excellent interface bonding is beneficial for deformation coordination and toughening of the C300/CoCrNi multilayer composites.

In order to analyze the contribution of each of the strengthening mechanisms in depth, the relevant theoretical calculations were introduced. The influence of the strengthening mechanism can be expressed as:

$$\sigma_{0.2} = \sigma_0 + \Delta\sigma_{refin} + \Delta\sigma_{twin} + \Delta\sigma_{pre}$$

where σ_0 is the value that the original material contributes to the yield strength, $\Delta\sigma_{refin}$ is the value of grain refining, $\Delta\sigma_{twin}$ is the value of strain-induced twinning, and $\Delta\sigma_{pre}$ is the value of the nanometer precipitate.

$$\sigma_0 = f_{CoCrNi}\sigma_{CoCrNi} + f_{C300}\sigma_{C300}$$

where f_{CoCrNi} and f_{C300} are the volume fractions of CoCrNi and C300 in the composites, respectively; $f_{CoCrNi} = f_{C300} = 0.5$; and σ_{CoCrNi} and σ_{C300} are the yield strengths of the original materials.

$$\Delta\sigma_{refin} = f_{CoCrNi}K_{CoCrNi}\Big/d_{CoCrNi}^{1/2} + f_{C300}K_{C300}\Big/d_{C300}^{1/2}$$

where K_{CoCrNi} (Liu et al., 2020) and K_{C300} (Rack, 1978) are the Hall–Petch constants of CoCrNi and C300, respectively, and d_{CoCrNi} and d_{C300} are the average grain diameters of the CoCrNi alloy layer and C300 layer, respectively, where $d_{CoCrNi} = 5$ μm and $d_{C300} = 3$ μm.

$$\Delta\sigma_{twin} = f_{CoCrNi}K_{twin}\Big/d_{CoCrNi}^{1/2}$$

where K_{twin} is a constant, $K_{twin} = 357$ MPa $\mu m^{1/2}$ (the Hall–Petch constant for twinning, which is similar to that for slip in TWIP steel (Gutierrez-Urrutia and Raabe, 2011)).

$$\Delta\sigma_{pre} = f_{C300} \times \frac{Gb}{2\pi(\lambda - d)} \times \frac{1 + 1/(1-\nu)}{2} \times ln\left[\frac{\lambda - d}{2b}\right]$$

where G is the shear modulus, $G = 71$ GPa; b is the Burger vector, $b = 0.25$ nm; λ is the particle spacing distance between precipitates, $\lambda = 20$ nm; d is the diameter of the precipitates,

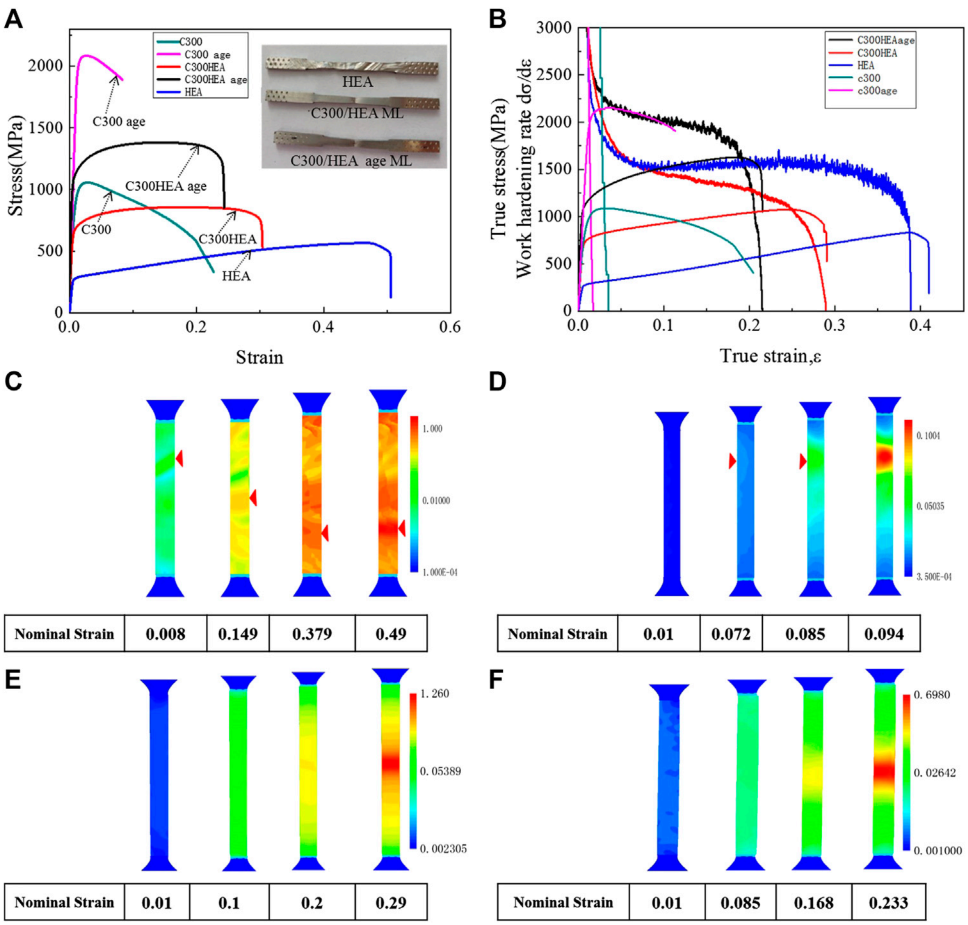

FIGURE 3 | (A) Stress–strain curve, **(B)** True stress–strain and work hardening rate curve, **(C–F)** Digital image correlation of the strain distribution, **(C)** CoCrNi alloy, **(D)** C300 aged, **(E)** rolled multilayer maraging/CoCrNi composite, and **(F)** aged multilayer maraging/CoCrNi composite.

$d = 5$ nm; and ν is Poisson's ratio, $\nu = 0.3$ (Zhu et al., 2014; Yang et al., 2015). The corresponding values for each item are shown in **Table 2**. The calculated values are approximated to the experimental results.

Figure 3C shows the strain evolution process of the individual CoCrNi alloy. It can be seen that multiple localized strain concentrations occur during the tensile deformation process, forming obvious multiple shear bands and localized necking phenomena. However, poor diffuse necking is inhibited because of the mutual competition of multiple strain localization zones, revealing superior strain-hardening capacity and fracture elongation. **Figure 3D** shows that an obvious localized strain concentration zone is formed at a strain of 0.085 and proceeds until fracture failure. That is to say, in C300 maraging steel it is easy to generate strain localization, leading to the formation of premature localized necking. The full-field strain distributions of the hot-rolled and aged multilayer C300/CoCrNi composites are shown in **Figures 3E,F**. The hot-rolled and aged multilayer metal composites both undergo a prolonged uniform plastic deformation stage until the strain concentration points reach 0.2 and 0.168, respectively. Finally, an obvious strain localization zone is located in the middle of the multilayer metal composites, resulting in fracture failure with a slight localized necking. That is to say, the C300/CoCrNi multilayer composites can integrate the advantages of the individual layers, effectively delaying the localized necking of

TABLE 2 | The contributions of grain refining, strain-induced twinning, and nanometer precipitate strengthening, and the calculated and experimental values of the yield stress.

Material sample	σ_0 (MPa)	$\Delta\sigma_{refin}$ (MPa)	$\Delta\sigma_{twin}$ (MPa)	$\Delta\sigma_{pre}$ (MPa)	Calculated value (MPa)	Experimental value (MPa)
Hot-rolled sample	518.7	77.3	79.5	—	675.5	666.8
Aged sample	518.7	81.3	79.5	388.9	1,068.4	1,060.9

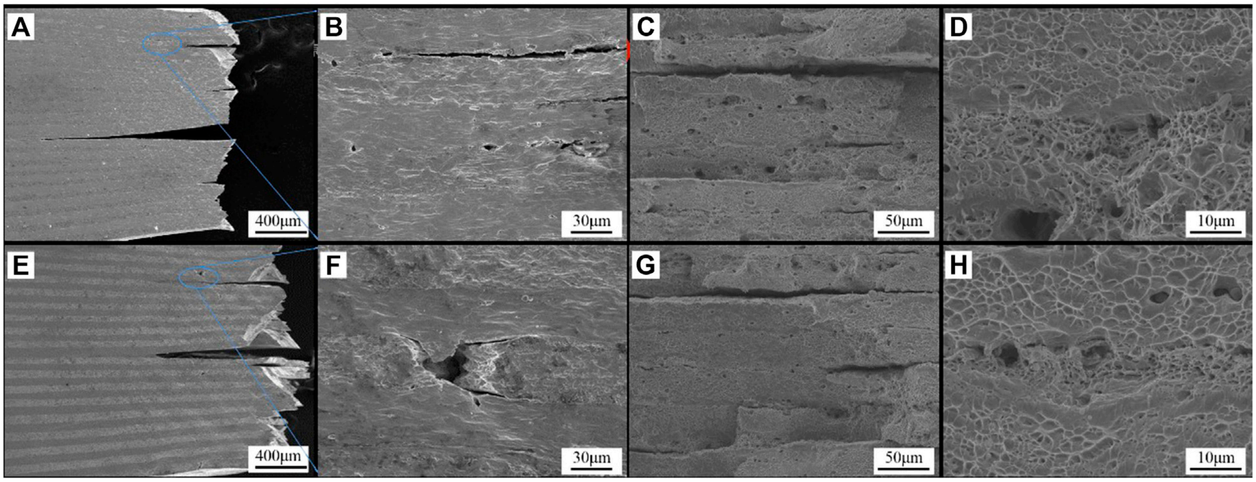

FIGURE 4 | (A–D) Fracture morphology of a hot-rolled multilayer maraging/CoCrNi composite, **(E–F)** fracture morphology of ageing treat multilayer maraging/CoCrNi composite.

C300 maraging steel and improving the yield strength of the CoCrNi alloy by reasonable interface bonding. Therefore, the C300/CoCrNi multilayer composite shows high yield strength and strain-hardening capacity.

Figure 4 shows the tensile fracture characteristics of the hot-rolled and aged multilayer metal matrix composites. The serious interface delamination cracks are located in the hot-rolled multilayer composites, as shown in **Figure 4A**, revealing a low interface bonding strength between the C300 and CoCrNi layers. The weak interface may be attributed to the high friction force and excessive interface inclusions during the hot-rolling process (Long et al., 2013; Li et al., 2008; Zhu et al., 2016). In addition, many discontinuous interface cracks and pores are located at the clad interface, as shown in **Figure 4B**; this can be attributed to the fractured interface inclusions. The above phenomenon reveals that the interface crack propagation of the multilayer composites experiences nucleation, growth, and convergence of microcracks (Liu et al., 2014). Also, the C300 and CoCrNi layers present coarse dimples with the same size of about 10 μm, which reveals a typical ductile fracture mode. Meanwhile, the interface transition zone possesses rather refined dimples with an average size of 2 μm, as shown in **Figure 4D**; these may be attributed to the ultrafine grains caused by severe plastic deformation. However, the aged C300/CoCrNi multilayer composites present slight and short interface delamination cracks, as shown in **Figure 4E**, which may be attributed to sufficient alloying element diffusion behavior at the clad interface during the long-time aging treatment (Seok et al., 2016). Moreover, the obvious tunnel cracks are located at the overall C300 maraging steel layer, as shown in **Figure 4F**. A relatively strong interface can effectively inhibit the strain concentration of the C300 layer, which is beneficial for enhancing the uniform plastic deformation capacity. Then the tunnel cracks cannot propagate into the overall sample owing to the existence of the CoCrNi alloy layer and strong interface, which can also delay the premature fracture failure of the C300 layer. Therefore, the slight interface delamination and formation of tunnel cracks are beneficial for toughening the multilayer composites. **Figures 4G,H** reveals the normal fracture characteristics of the C300/CoCrNi multilayer composites. Many bifurcated cleavage cracks are located at the C300 layer, indicating that the C300 layer can be toughened by forming multiple cracks. Compared with the hot-rolled sample, the aged C300 layer has many fine dimples, as shown in **Figure 4H**. That is to say, the nanoscale precipitates can play an important role in strengthening and toughening the multilayer composites.

CONCLUSION

In the present work, we design and fabricate a novel C300/CoCrNi multilayer composite by a vacuum hot-rolling and aging treatment. Herein, the ultimate tensile strength of the multilayer metal composites can reach 1,380 MPa with a high fracture elongation of 24%, as well as superior uniform elongation of 15.7%. This indicates an excellent strengthening–toughening behavior. The aging treatment eliminates the rolling friction stress and promotes diffusion of the alloying element at the clad interface, realizing strong interface bonding. The clad interface and tunnel crack play an important role in toughening the C300/CoCrNi multilayer composites. That is to say, a strong clad interface and CoCrNi layer with a high strain-hardening capacity can effectively delay premature localized necking and fracture failure of the C300 layer, achieving a superior strength–ductility balance.

DATA AVAILABILITY STATEMENT

The original contributions presented in the study are included in the article/Supplementary Material, further inquiries can be directed to the corresponding authors.

AUTHOR CONTRIBUTIONS

CX Writing: original draft preparation, conceptualization. YG Data curation. WFang Investigation. XZ Methodology, Validation. BXL Writing: reviewing and editing. JF Methodology. FY Funding acquisition. All authors contributed to the article and approved the submitted version.

FUNDING

The Joint Fund for Steel Research of National Natural Science Foundation of China and Baowu Steel Group Corporation Limited (No. U1860114), the foundation strengthening program (No. 2019-JCJQ-142) the National Natural Science Foundation of China (No. 51705129). The funder was not involved in the study design, collection, analysis, interpretation of data, the writing of this article, or the decision to submit it for publication.

ACKNOWLEDGMENTS

This work is supported financially by the National Natural Science Foundation of China (NSFC) under grant no. 51701061, the Joint Fund for Steel Research of the National Natural Science Foundation of China and Baowu Steel Group Corporation Limited (no. U1860114), the Foundation Strengthening Program (no.2019-JCJQ-142), and the National Natural Science Foundation of China (no. 51705129).

REFERENCES

Chang, R. B., Fang, W., Yu, H. Y., Bai, X., Zhang, X., Liu, B. X., et al. (2019). Heterogeneous banded precipitation of (CoCrNi)93Mo7 medium entropy alloys towards strength–ductility synergy utilizing compositional inhomogeneity. *Scripta Mater.* 172, 144–148. doi:10.1016/j.scriptamat.2019.07.026

Ding, H., Cui, X., Gao, N., Sun, Y., Zhang, Y., Huang, L., et al. (2021). Fabrication of (TiB/Ti)-TiAl composites with a controlled laminated architecture and enhanced mechanical properties. *J. Mater. Sci. Technol.* 62, 221–233. doi:10.1016/j.jmst.2020.06.011

Ding, H., Cui, X., Xu, C., Li, A., Geng, L., Fan, G., et al. (2018). Fabrication and mechanical characteristics of multi-laminated aluminum matrix composites reinforcedby continuous basalt fibers. 54, 1171–1178. doi:10.11900/0412.1961.2017.00530

Grassel, O., Kruger, L., Frommeyer, G., and Meyer, L. W. (2000). High strength Fe-Mn-(Al, Si) TRIP/TWIP steels development - properties- application. *Int. J. Plast.* 16, 1391–1409. doi:10.1016/S0749-6419(00)00015-2

Gutierrez-Urrutia, I., and Raabe, D. (2011). Dislocation and twin substructure evolution during strain hardening of an Fe–22wt.% Mn–0.6wt.% C TWIP steel observed by electron channeling contrast imaging. *Acta Mater.* 59, 6449–6462. doi:10.1016/j.actamat.2011.07.009

Gutierrezurrutia, I., and Raabe, D. (2011). Dislocation and twin substructure evolution during strain hardening of an Fe-22 wt.% Mn-0.6 wt.% C TWIP steel observed by electron channeling contrast imaging. *Acta Mater.* 59, 6449–6462. doi:10.1016/j.actamat.2011.07.009

He, G., Zhao, Y., Gan, B., Sheng, X., Liu, Y., and Tan, L. (2020). Mechanism of grain refinement in an equiatomic medium-entropy alloy CrCoNi during hot deformation. *J. Alloys Compd.* 815, 152382. doi:10.1016/j.jallcom.2019.152382

Inoue, J., Nambu, S., Ishimoto, Y., and Koseki, T. (2008). Fracture elongation of brittle/ductile multilayered steel composites with a strong interface. *Scripta Mater.* 59,1055–1058. doi:10.1016/j.scriptamat.2008.07.020

Jing, Y. A., Qin, Y., Zang, X., Shang, Q., and Hua, S. (2014). A novel reduction-bonding process to fabricate stainless steel clad plate. *J. Alloys Compd.* 617, 688–698. doi:10.1016/j.jallcom.2014.07.186

Kang, J. Y., Kim, J. G., Kim, S. K., Chin, K. G., Lee, S., and Kim, H. S. (2016). Outstanding mechanical properties of high-pressure torsion processed multiscale TWIP-cored three layer steel sheet. *Scripta Mater.* 123, 122–125. doi:10.1016/j.scriptamat.2016.06.009

Lesuer, D. R., Syn, C. K., Sherby, O. D., Wadsworth, J., Lewandowski, J. J., and Hunt, W. H. (1996). Mechanical behaviour of laminated metal composites. *Int. Mater. Rev.* 41, 169–197. doi:10.1179/imr.1996.41.5.169

Li, L., Nagai, K., and Yin, F. (2008). Progress in cold roll bonding of metals. *Sci. Technol. Adv. Mat.* 9, 023001. doi:10.1088/1468-6996/9/2/023001

Liu, B. X., An, Q., Yin, F. X., Wang, S., and Chen, C. X. (2019). Interface formation and bonding mechanisms of hot-rolled stainless steel clad plate. *J. Mater. Sci.* 54, 11357–11377. doi:10.1007/s10853-019-03581-x

Liu, B. X., Huang, L. J., Geng, L., Wang, B., and Cui, X. P. (2014). Fracture behaviors and microstructural failure mechanisms of laminated Ti–TiBw/Ti composites. *Mater. Sci. Eng.* 611, 290–297. doi:10.1016/j.msea.2014.05.089

Liu, X., Zhang, M., Ma, Y., Dong, W., Li, R., Lu, Y., et al. (2020). Achieving ultrahigh strength in CoCrNi-based medium-entropy alloys with synergistic strengthening effect. *Mater. Sci. Eng. A.* 776, 139028. doi:10.1016/j.msea.2020.139028

Long, L. I., Xin-Jin, Z., Hui-Yun, L. I. U., and Fu-Xing, Y. I. N. (2013). Formation mechanism of oxide inclusion on the interface of hot-rolled stainless steel clad plates. *J. Iron Steel Res.* 25, 43–47. doi:10.13228/j.boyuan

Miao, J., Slone, C. E., Smith, T. M., Niu, C., Bei, H., Ghazisaeidi, M., et al. (2017). The evolution of the deformation substructure in a Ni-Co-Cr equiatomic solid solution alloy. *M. Acta Mater.* 132, 35–48. doi:10.1016/j.actamat.2017.04.033

Ojima, M., Inoue, J., Nambu, S., Xu, P., Akita, K., Suzuki, H., and Koseki, T. (2012). Stress partitioning behavior of multilayered steels during tensile deformation measured by *in situ* neutron diffraction. *Scripta Mater.* 66, 139–142. doi:10.1016/j.scriptamat.2011.10.018

Rack, H. J. (1978). Age hardening-grain size relationships in 18Ni maraging steels. *Mater. Sci. Eng.* 34, 263–270. doi:10.1016/0025-5416(78)90058-7

Seok, M. Y., Lee, J. A., Lee, D. H., Ramamurty, U., Nambu, S., Koseki, T., et al. (2016). Decoupling the contributions of constituent layers to the strength and ductility of a multi-layered steel. *Acta Mater.* 121, 164–172. doi:10.1016/j.actamat.2016.09.007

Slone, C. E., Chakraborty, S., Miao, J., George, E. P., Mills, M. J., and Niezgoda, S. R. (2018). Influence of deformation induced nanoscale twinning and FCC-HCP transformation on hardening and texture development in medium-entropy CrCoNi alloy. *Acta Mater.* 158, 38–52. doi:10.1016/j.actamat.2018.07.028

Slone, C. E., Chakraborty, S., Miao, J., George, E. P., Mills, S. R., and Niezgoda, M. J. (2018). Influence of deformation induced nanoscale twinning and FCC-HCP transformation on hardening and texture development in medium-entropy CrCoNi alloy. *Acta Mater.* 158, 38–52. doi:10.1016/j.actamat.2018.12.015

Slone, C. E., Miao, J., George, E. P., and Mills, M. J. (2019). Achieving ultra-high strength and ductility in equiatomic CrCoNi with partially recrystallized microstructures. *Acta Mater.* 165, 496–507. doi:10.1016/j.actamat.2018.12.015

Wu, Z., Bei, H., Pharr, G. M., and George, E. P. (2014). Temperature dependence of the mechanical properties of equiatomic solid solution alloys with face-centered cubic crystal structures. *Acta Mater.* 81, 428–441. doi:10.1016/j.actamat.2014.08.026

Yang, S., Peng, Y., Zhang, X. M., and Tian, Z. L. (2015). Phase transformation and its effect on mechanical properties of C300 weld metal after aging treatment at different temperatures. *J. Iron Steel Res. Int.* 6, 527–533. doi:10.1016/S1006-706X(15)30036-4

Yin, F. X., Li, L., Tanaka, Y., Kishimoto, S., and Nagai, K. (2013). Hot rolling bonded multilayered composite steels and varied tensile deformation behaviour. *Mater. Sci. Technol.* 28, 783–787. doi:10.1179/1743284711y.0000000116

Yu, W. X., Liu, B. X., Cui, X. P., Dong, Y. C., Zhang, X., He, J. N., et al. (2018). Revealing extraordinary strength and toughness of multilayer TWIP/Maraging steels. *Mater. Sci. Eng. A*. 727, 70–77. doi:10.1016/j.msea.2018.04.097

Zhang, S., Xiao, H., Xie, H., and Gu, L. (2014). The preparation and property research of the stainless steel/iron scrap clad plate. *J. Mater. Process. Technol.* 214, 1205–1210. doi:10.1016/j.jmatprotec.2014.01.006

Zhu, F., Yin, Y. F., and Faulkner, R. G. (2014). Microstructural control of maraging steel C300. *Mater. Sci. Technol.* 27, 395–405. doi:10.1179/026708309x12506933873503

Zhu, Z., He, Y., Zhang, X., Liu, H., and Li, X. (2016). Effect of interface oxides on shear properties of hot-rolled stainless steel clad plate. *Mat. Sci. Eng. a-Struct.* 669, 344–349. doi:10.1016/j.msea.2016.05.066

Conflict of Interest: The authors declare that the research was conducted in the absence of any commercial or financial relationships that could be construed as a potential conflict of interest.

This study received funding from the Joint Fund for Steel Research of the National Natural Science Foundation of China and Baowu Steel Group Corporation Limited.